Supplement of Atmos. Chem. Phys., 21, 1173–1189, 2021
https://doi.org/10.5194/acp-21-1173-2021-supplement


Atmospheric Chemistry and Physics
Open Access
EGU

*Supplement of*

# Spatiotemporal variation and trends in equivalent black carbon in the Helsinki metropolitan area in Finland

**Krista Luoma et al.**

*Correspondence to:* Krista Luoma (krista.q.luoma@helsinki.fi)

**Supplement of "Spatiotemporal variation and trends of equivalent black carbon in the Helsinki Metropolitan area in Finland".**

## S1 Meteorological parameters

The seasonal variation of the temperature (T), wind speed (WS), and mixing height (MH) in the HMA during 2009–2018 are presented in Figs. S1a–c, and the time series of these parameters are presented in Figs. S1d–f. The variation of WS and MH is presented in more detail in Fig. S2, which presents the diurnal variation of the WS and MH separately for the cold (November – March) and the warm (May – September) seasons. The T and WS data presented in the supplementary were measured at weather observation site in Helsinki and the MH was a modelled value for southern Finland (see Sect. 2.4).

We applied the trend analysis for the meteorological parameters as well, but we did not observe statistically significant long-term trends for the time series of T, WS, or MH (Figs. S1d–e). The trends were studied also separately for each season, which were spring (March – May), summer (June – August), autumn (September – November), and winter (December – February). However, this analysis did not yield any statistically significant trends either.

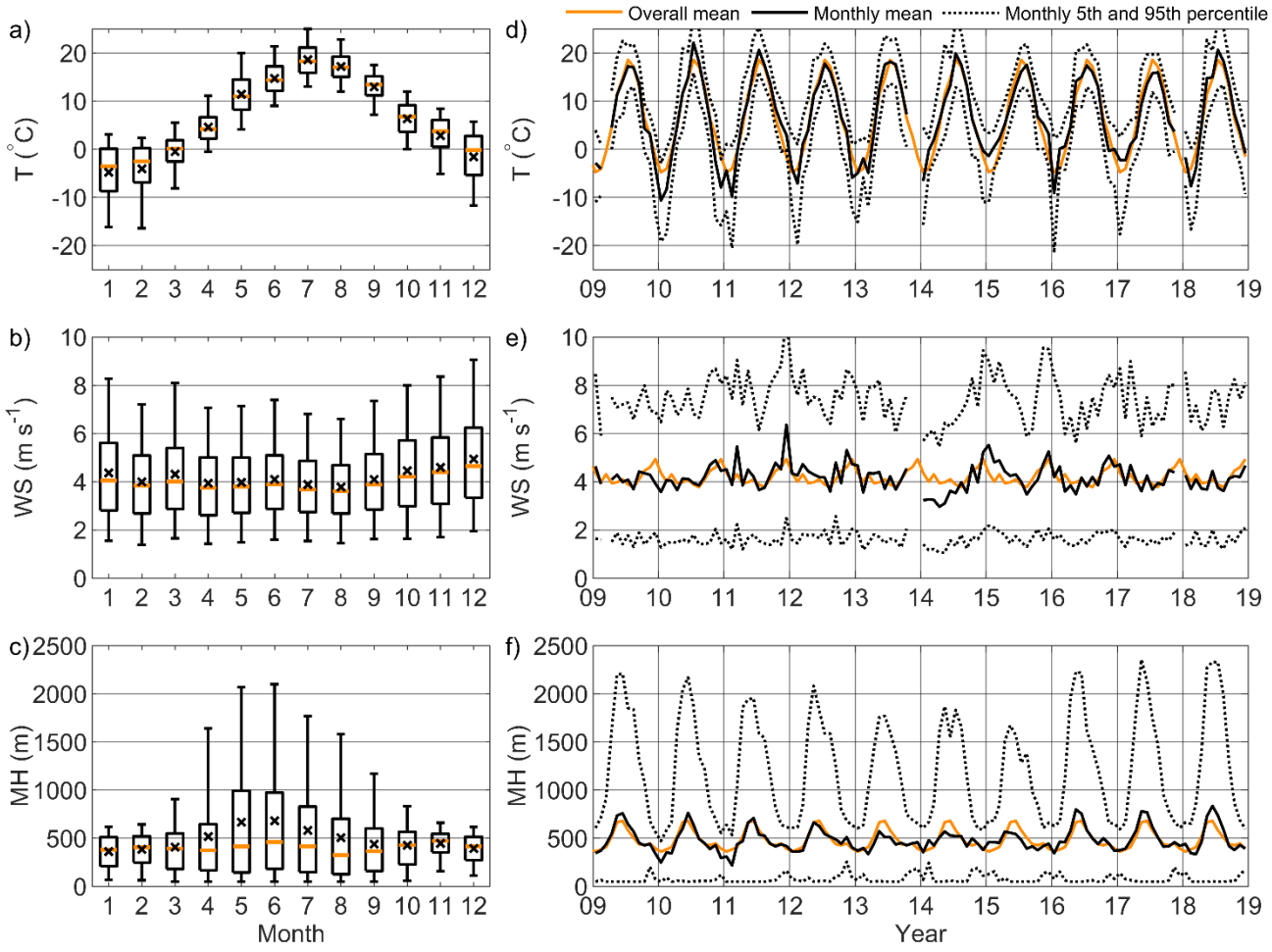


**Figure S1: Monthly statistics of different meteorological parameters on the left panel: a) temperature (T), b) wind speed (WS), and c) mixing height (MH). The orange line in the middle of each box represents the median, the edges of the boxes represent the 25$^{th}$ and 75$^{th}$ percentiles, and the whiskers represent the 5$^{th}$ and 95$^{th}$ percentiles. The black cross is the arithmetic mean. On the right panel are the time series of d) T, e) WS, and f) MH. The statistical values were determined from 1 h averaged data.**

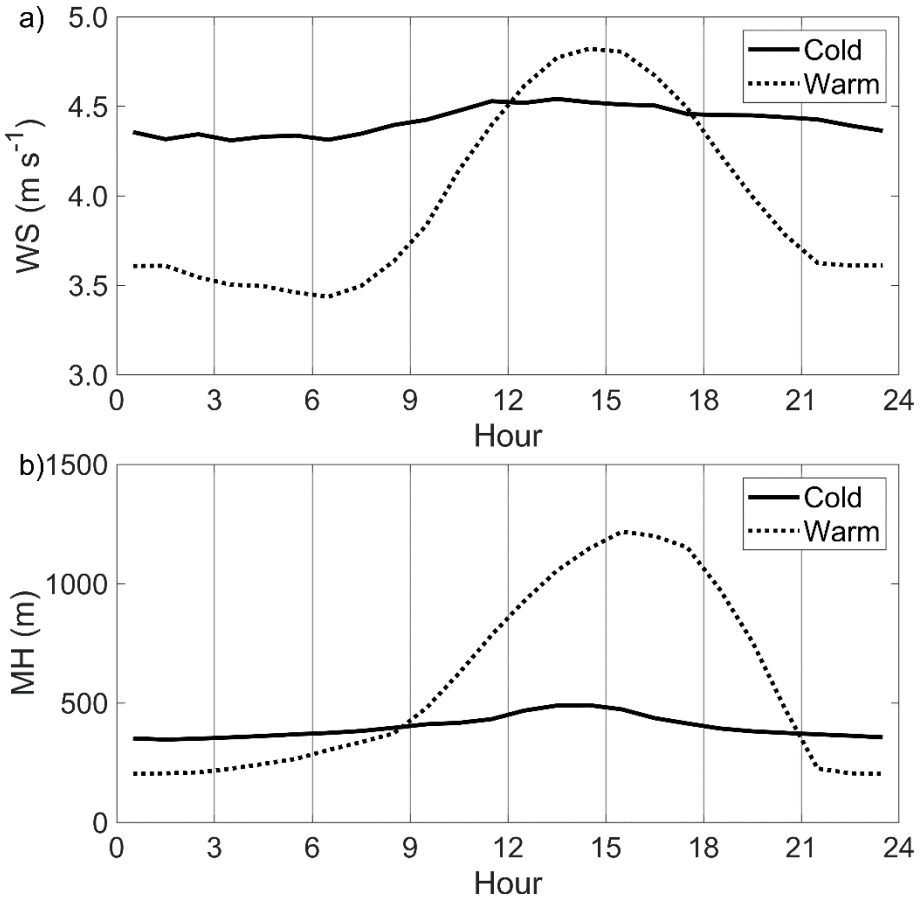


**Figure S2: Mean diurnal variation of a) wind speed (WS) and b) mixing height (MH) for the cold (November – March) and warm (May – September) seasons. The diurnal variations were calculated from 1 h mean values.**

## S2 Detailed description of the measurement sites

This section presents more detailed descriptions and aerial photos (size scale is the same in all the subfigures) from each site. The coordinates for each station are given in Table S1, which also lists all the used instruments for measuring equivalent black carbon concentration (eBC), the mass of particles smaller than 2.5 µm ($PM_{2.5}$), and $NO_x$ concentration.

**Table S1: Detailed information about the eBC measurements at the different stations. FH 62 I-R determines the aerosol mass concentration by measuring the attenuation of β-radiation, TEOM uses an oscillating microbalance method and Grimm measures the mass by optical means.**

| Station | Coordinates | eBC instrument | $PM_{2.5}$ instrument | $NO_x$ instrument | Operator |
|---|---|---|---|---|---|
| TR1 | 60°10’10.6’’N 24°56’21.5’’E | MAAP | FH 62 I-R | Horiba APNA 370 | HSY |
| TR2 | 60°11’47.1’’N 24°57’07.4’’E | MAAP | TEOM 1405, TEOM 1400 AB | Horiba APNA 370 | HSY |
| TR3 | 60°11’24.1’’N 24°54’57.7’’E | MAAP | TEOM 1400 AB | Horiba APNA 370 | HSY |
| TR4 | 60°14’30.7’’N 25°01’32.5’’E | MAAP | TEOM 1400 AB | Horiba APNA 370 | HSY |
| TR5 | 60°17’23.8’’N 25°02’22.4’’E | MAAP | TEOM 1400 AB, TEOM 1405 | Horiba APNA 370 | HSY |
| TR6 | 60°13’13.0’’N 24°48’40.9’’E | MAAP | FH 62 I-R | Horiba APNA 370 | HSY |
| DH1 | 60°13’26.5’’N 25°06’09.4’’E | MAAP | Grimm 180 | Horiba APNA 370 | HSY |
| DH2 | 60°18’43.4’’N 25°00’39.9’’E | MAAP | FH 62 I-R | Horiba APNA 360 | HSY |
| DH3 | 60°14’21.9’’N 24°48’49.4’’E | MAAP | FH 62 I-R | Horiba APNA 360 | HSY |
| DH4 | 60°19’53.2’’N 25°04’33.2’’E | MAAP and AE33 | FH 62 I-R | Horiba APNA 360 | HSY |
| DH5 | 60°17’30.2’’N 25°06’46.3’’E | AE33 | FH 62 I-R | Horiba APNA 370 | HSY |
| UB1 | 60°11’14.5’’N 24°57’02.3’’E | MAAP | TEOM 1405, TEOM 1400 AB | Horiba APNA 370, Thermo 42i | HSY |
| UB2 | 60°12’10.4’’N 24°57’40.4’’E | MAAP | TEOM 1405D | API 200AU, Horiba APNA 360 | FMI, UHEL |
| RB1 | 60°18’51.7’’N 24°41’04.6’’E | MAAP | FH 62 I-R | Horiba APNA 370 | HSY |
| RB2 | 61°50’47.5’’N 24°17’40.1’’E | MAAP and AE31 | Cascade-impactor and manual weightings | TEI 42CTL and 42iTL with photolytic converter | UHEL |

30

**S2.1 Traffic sites**

Figure S3 presents the aerial photos from each traffic site (TR) and it also shows the names of the closest streets or roads.

TR1 was located right in the city center and the station represented the concentration level that pedestrians are exposed to in the city center. TR2 and TR3 were located in street canyons, where tall buildings frame the streets. TR2 was located next to Mäkelänkatu, which is one of the main streets leading to Helsinki city center, and TR3 was located in the northern part of Mannerheimintie, another main street to Helsinki city center. In addition to passenger cars, many busses (heavy-duty) bypass TR2 and TR3.

While TR1, TR2, and TR3 were in or close to the Helsinki city center, TR4 was located next to a ring road, Kehä I, which is a highway going around the Helsinki city. The station represented the concentration level on walkways and bus stops that are next to major roads.

TR5 and TR6 were located close to busy streets and intersections in the city centers of Vantaa and Espoo, respectively. These city centers were not as large as the city center of Helsinki, but there were still busy roads and apartment buildings. As seen in Fig. 1, TR5 and TR6 were closer to the detached housing areas than the other TR stations.

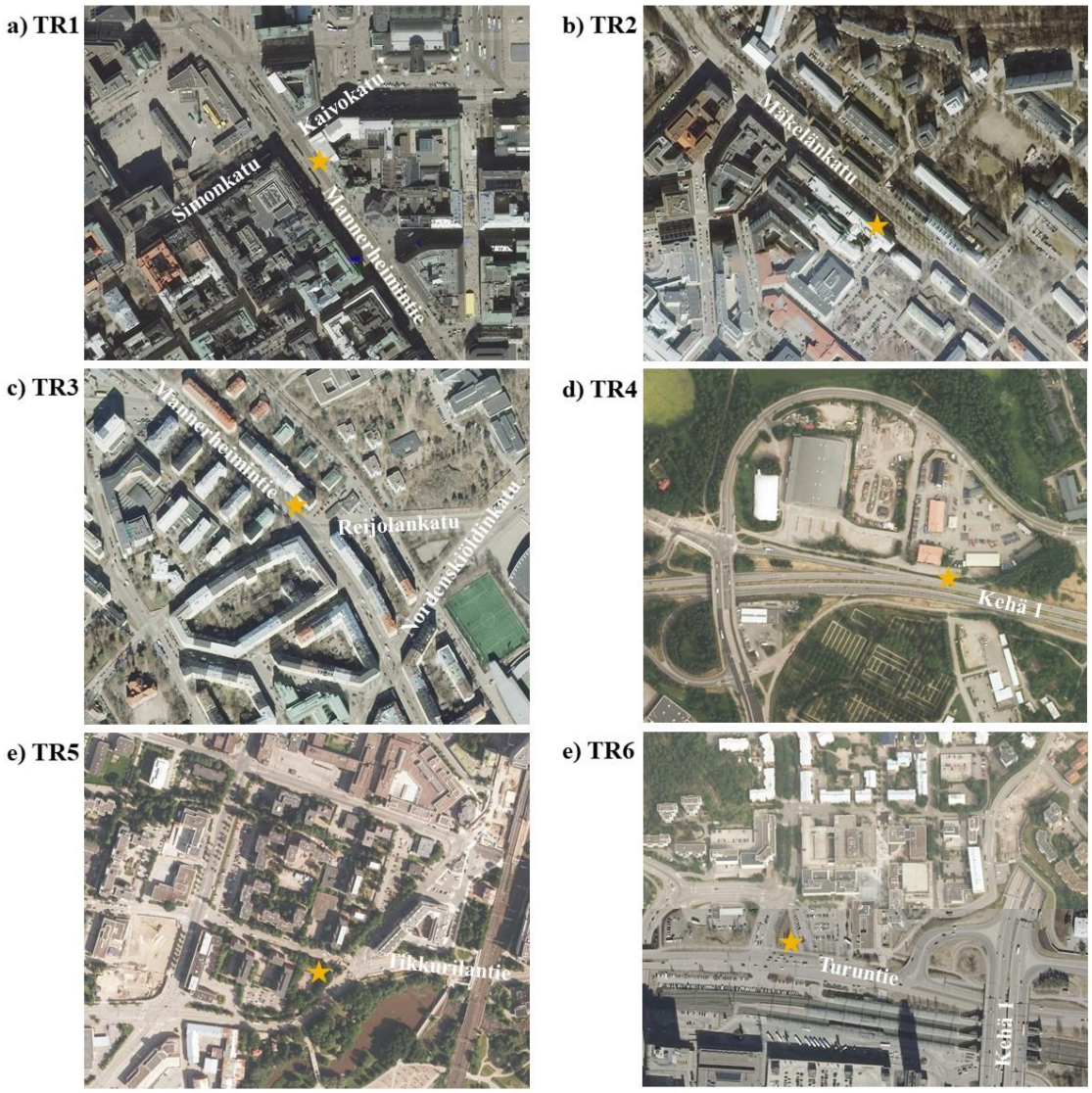


**Figure S3: Aerial pictures of the traffic sites. The location of the station is marked with a star. The size range on the East – West direction is about 600 m and on the North – South direction around 460 m. The pictures are modified (street names and the location of the station were added) from the orthophotos provided by the National Land Survey of Finland (02/2020).**

### S2.2 Detached housing sites

Figure S4 presents the aerial photos from the detached housing sites (DH). DH1, DH2, DH3, DH4, and DH5 were located in Vartiokylä, Ruskeasanta, Lintuvaara, Rekola, and Itä-Hakkila, respectively.


**Figure S4: Aerial pictures of the stations located in the detached house areas. The location of the station is marked with a star. The size ranges are the same as in Fig. S3. The pictures are modified (location of the station was added) from the orthophotos provided by the National Land Survey of Finland (02/2020).**

### S2.3 Background sites

Figure S5 presents the aerial photos from both urban background (UB) and regional background (RB) sites.

UB1 was located in the Kallio district next to a sports field and close to Helsinginkatu, a moderately busy street, where the average working day traffic count was about 5 000 vehicles per day (5 % heavy-duty). The area consisted mostly of apartment buildings. UB2 was located in Kumpula, in the campus of the University of Helsinki. There was a busy street, Hämeentie, located behind a 200 m wide forest band. The traffic count at Hämeentie was about 40 000 vehicles per day.

RB1 was located in Luukki, which is a rural area in Espoo about 20 km away from the Helsinki city center. RB2 was located almost 200 km away from Helsinki in Hyytiälä in the middle of a boreal forest.

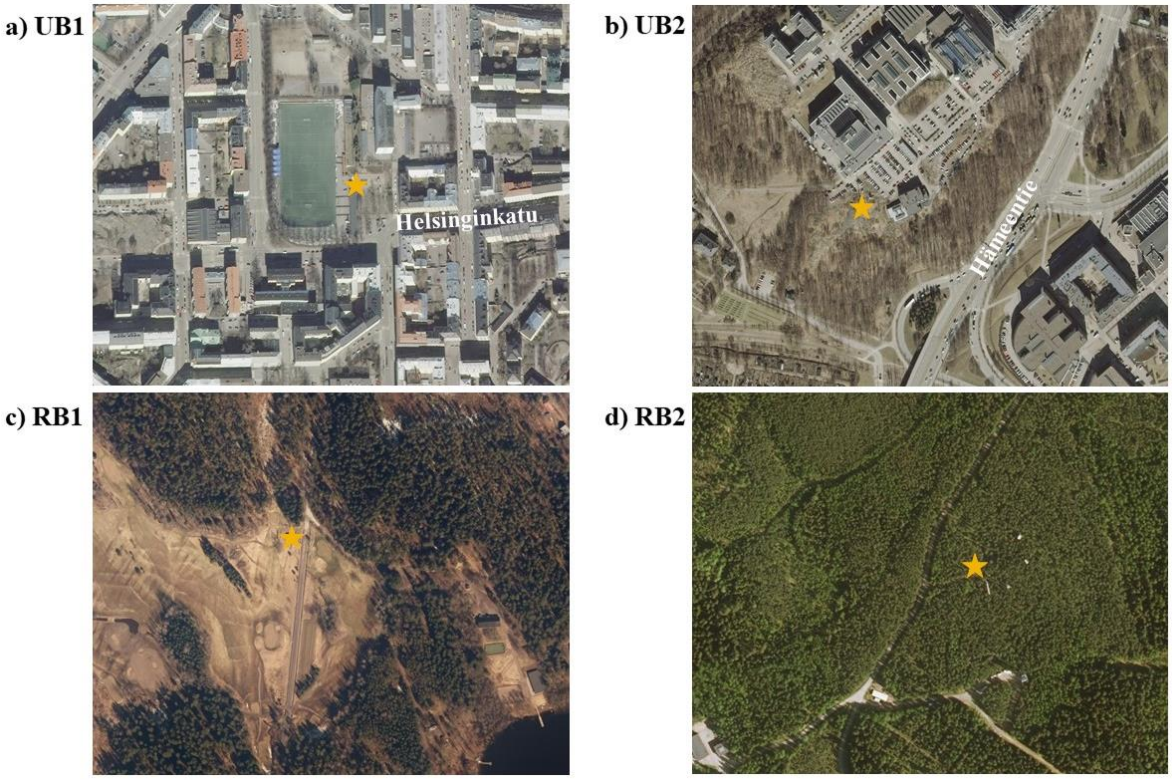


**Figure S5: Aerial pictures of the background stations. The location of the station is marked with a star. The size ranges are the same as in Fig. S3. The pictures are modified (location of the station was added) from the orthophotos provided by the National Land Survey of Finland (02/2020).**

## S3 AE31 and MAAP comparison at RB2

The comparison between the Aethalometer model AE31 and Multi-Angle Absorption Photometer (MAAP) is shown in Fig. S6. The comparison includes data measured during July 2013 – December 2018, when the MAAP was measuring in parallel with the AE31. The BC data measured with the AE31 at wavelength 880 nm was corrected by using the correction algorithm described by Virkkula et al. (2007) and the data was compared against the concentration measured by MAAP at wavelength 637 nm.

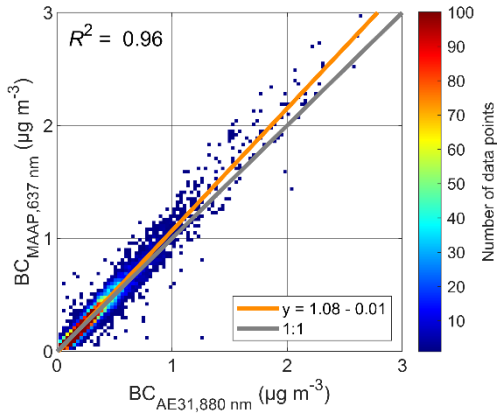


**Figure S6: Relation between eBC measured by the MAAP and the AE31 at RB2. The color of the grid points indicates the number of data points. The orange line is the linear fit and the grey line is the 1:1 line. Due to the large data set, the standard errors of the slope and intercept were small, 0.0013 and 0.0004, respectively. The size of each grid point is 0.03 µg $m^{-3}$ in both x- and y-directions (i.e., there are 100 x 100 grid points in total).**

## S4 Correlation between eBC and other air pollutants

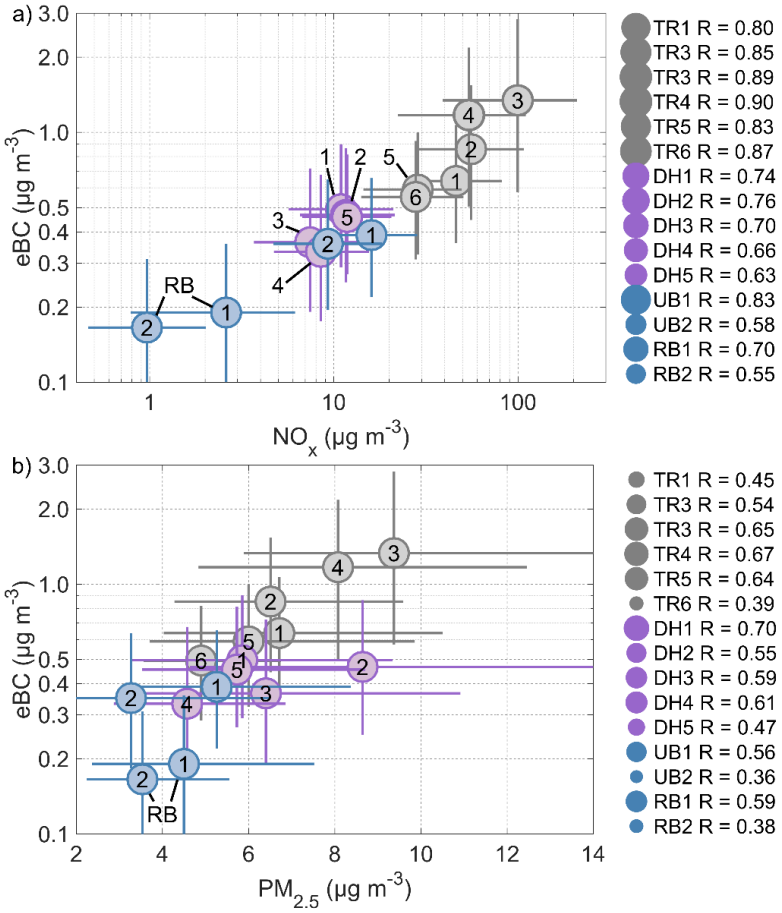


**Figure S7: Relation between a) eBC and $NO_x$ concentration, and b) eBC and $PM_{2.5}$ concentration. The circles mark the median eBC, $NO_x$ and $PM_{2.5}$ values and the whiskers are the 25th and 75th percentiles of all the available data for each station. The grey markers represent the traffic stations, purple represent the detached housing stations, and the blue markers represent the background sites. The correlations between the variables at each station are presented on the right side, where the marker size represents the correlation coefficient. The correlation coefficients of the median values were *R* = 0.95 and *R* = 0.78 for the a) and b) subfigures, respectively. Note that the y-axis and also the x-axis in a) are in logarithmic scale.**

## S5 Trends at TR3

The eBC concentration at TR3 showed clear decrease between the years 2010 and 2015. However, since there were only two years of measurements, we could not apply the seasonal Kendall test to see if there was a statistically significant decreasing trend. Therefore, we ran a Mann-Whitney U-test for the TR3 air pollution data to see if the difference in the median values between these two years (1.83 and 1.00 μg $m^{-3}$ for 2010 and 2015, respectively) was statistically significant. The test showed a statistically significant difference (p-value << 0.01) between the median values of the annual eBC concentration. According to the annual medians, the median decreased 0.17 μg $m^{-3}$ $yr^{-1}$ (-12 % $yr^{-1}$). With a similar analysis, we got a decrease of 8 μg $m^{-3}$ $yr^{-1}$ (-8 % $yr^{-1}$) and -0.6 μg $m^{-3}$ $yr^{-1}$ (-7 % $yr^{-1}$) for the $NO_x$ and $PM_{2.5}$ data.

One reason for the decrease in the concentrations of different air pollutants is probably the decrease in traffic counts next to the site. In 2010 the traffic count on the street next to TR3 was estimated to be 44 400 vehicles per weekday and in 2015 the estimated traffic count had decreased to 33 500 vehicles per weekday.

In addition to the traffic count, also different meteorological conditions might explain the notable decrease in the air pollutant concentrations. The differences in the meteorological parameters (T and WS) in 2010 and 2015 are compared in Fig. S8. The figure shows that in 2010, when the eBC concentration was notably higher, the T was actually much lower during the winter in 2010 than in 2015. Also, the WS was lower during the winter in 2010 compared to 2015. During summer, the T was a bit

higher in 2010 than in 2015. Teinilä et al., (2019) showed that the most important meteorological parameters explaining the eBC concentration are the T and WS, so that the highest pollutant concentrations are measured during calm winds when the temperature is either cold or hot. Therefore, the annual variation of T and WS most probably explain at least part of the high concentrations measured at TR3 in 2010. This example shows that the meteorological parameters might have a big effect on the year-to-year-variation of the air pollutant concentrations.

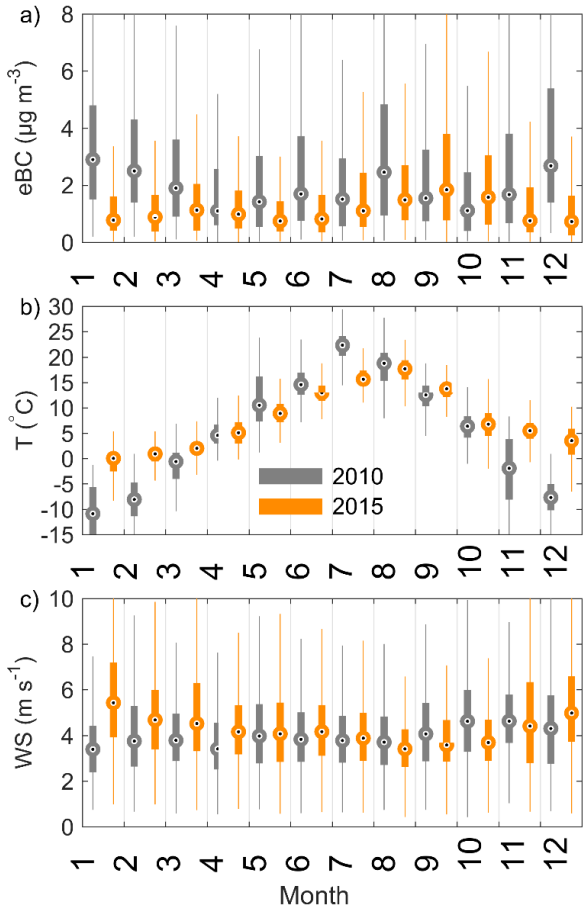


**Figure S8: Statistics of the a) eBC concentration at TR3, b) temperature (T), and c) wind speed (WS) in Helsinki in 2010 and 2015.**

## S6 Traffic counts in the HMA

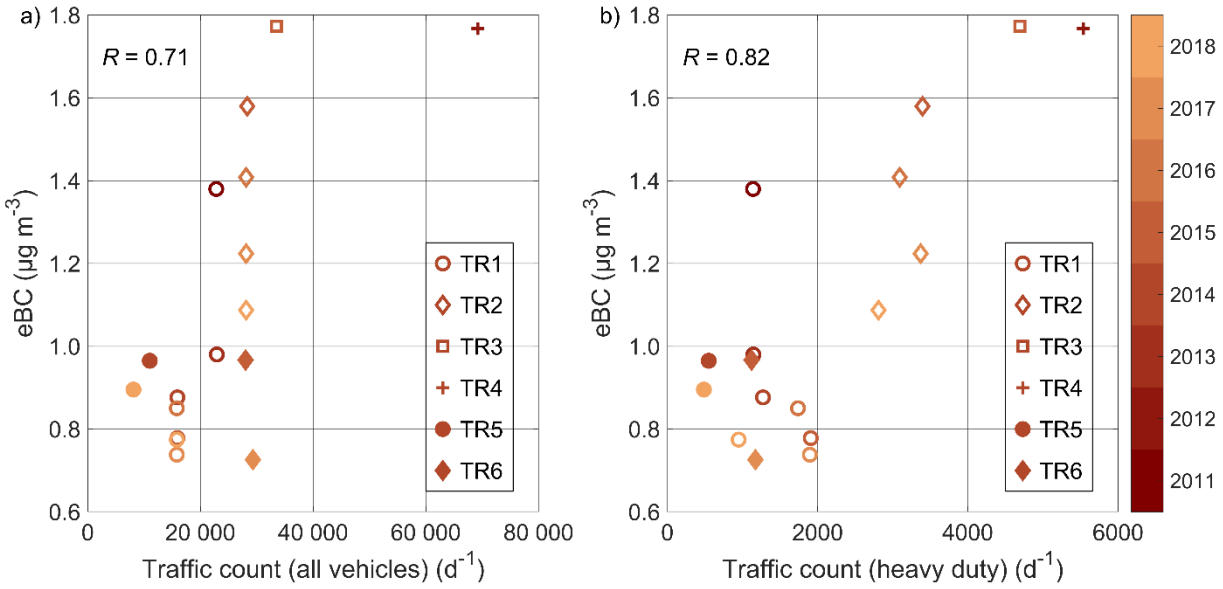


**Figure S9: Relation between a) eBC concentration and total traffic count, and b) eBC concentration and the traffic count of heavy-duty vehicles for each station and year separately. The eBC values are annual means, which were determined for weekdays only. The traffic counts are estimates for the closest street on a weekday. The estimates were provided in the yearly traffic reports by the city of Helsinki. The data from TR3 in 2010 and TR5 in 2016 were omitted, since there was no estimation for the heavy-duty traffic count.**

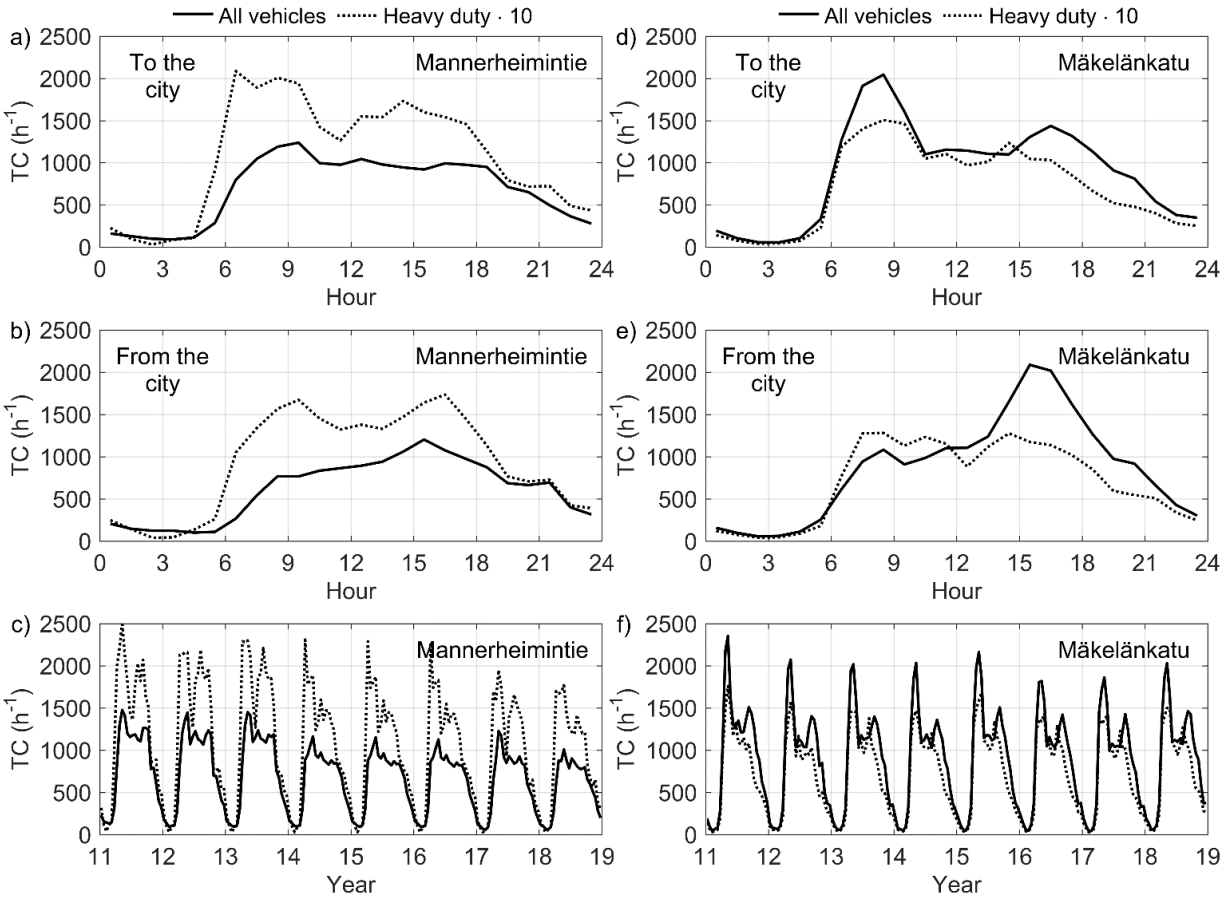


**Figure S10: Traffic counts (TC) at a) – c) Mannerheimintie and d) – e) Mäkelänkatu streets. Here, the measurement point at Mannerheimintie was located about 2 km North of TR3 and the measurement point at Mäkelänkatu was located about 400 m North-West of TR2, so the TC does not necessarily represent the traffic at TR3 and TR2. Note that the TC of heavy-duty is multiplied by 10 to make the comparison easier. Mean TC for each hour in the traffic lanes that lead towards the city centre are presented in subfigures a) and d), and subfigures b) and e) present the diurnal variation of TC in the traffic lanes that lead away from the city centre. Subfigures c) and f) present the diurnal TC for each year. The TC data was provided by the Helsinki Region Infoshare (06/2019).**

## S5 Temporal variation

In this section, we provide supplementary material and more detailed information about the variation of eBC. Figure S11 is similar to Fig. 2, but here the spatial variation is presented separately for the cold and the warm seasons. The seasonal variation and the diurnal variation for each station separately are presented in Figs. S12 and S13, respectively.

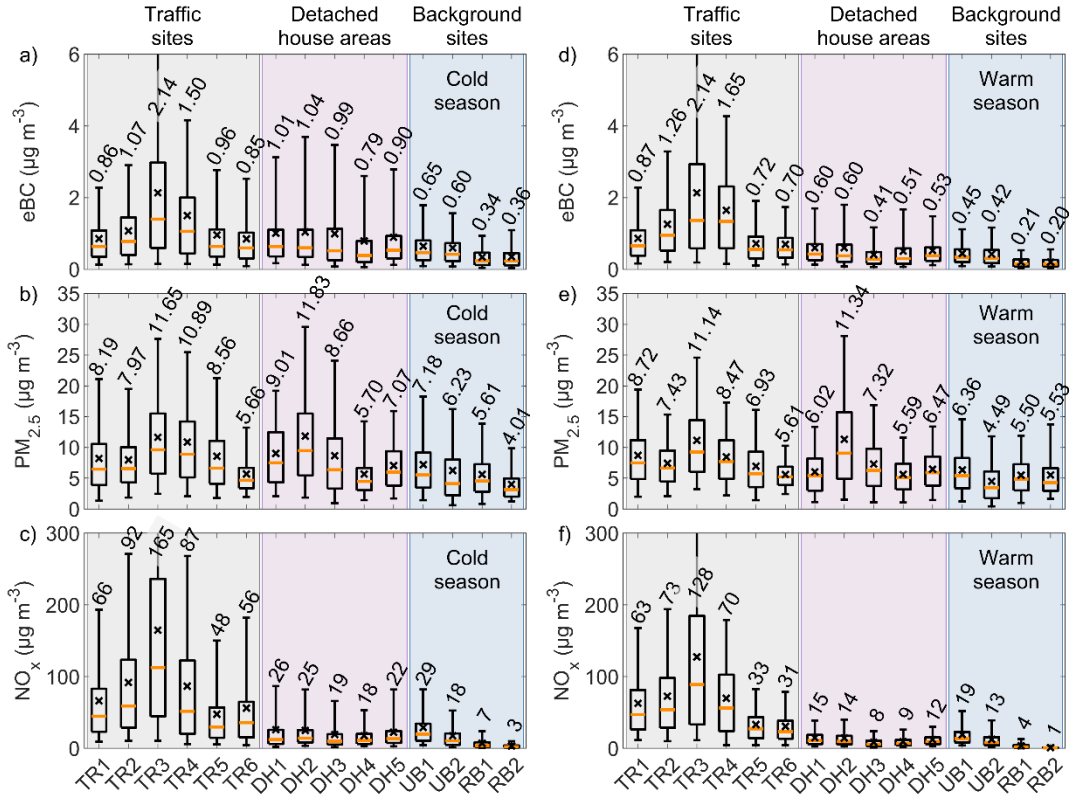


**Figure S11: Statistics of the eBC, $PM_{2.5}$, and $NO_x$ concentrations at each station separated for the cold (November – March; left column) and warm (May – September; right column) seasons. The boxplots were calculated from 1 h mean values. The explanation for the boxes are the same as in Fig. S1. The mean values are reported above each box. The background color represents the station type: gray for the TR sites, purple for the DH sites, and blue for the background (UB and RB) sites.**

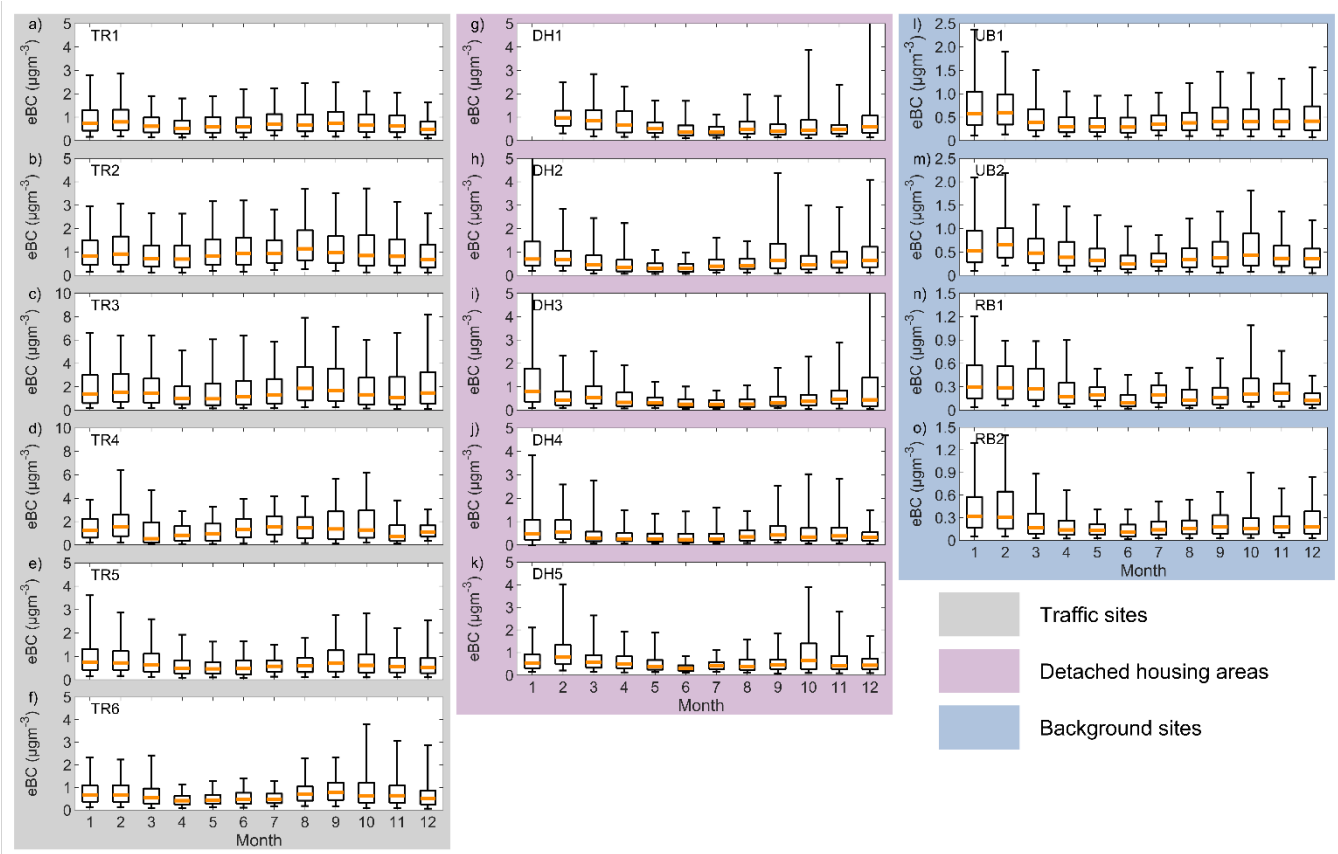


**Figure S12: Seasonal variation for each station separately. The explanation for the boxes is the same as in Fig. S1.**

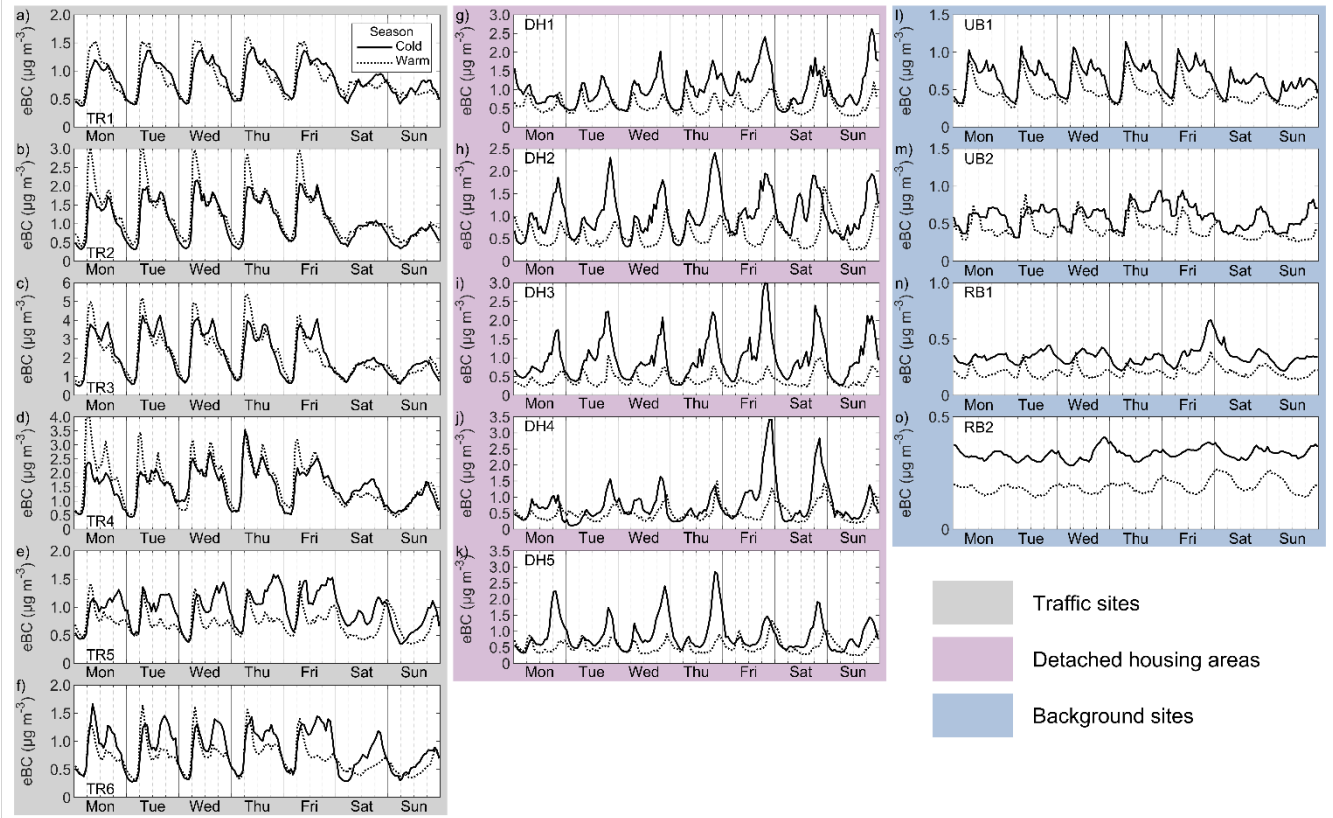


**Figure S13: Similar to Fig. 6, but here the diurnal variation is presented separately at each site.**

Figure S14 presents the diurnal variation of the eBC/$PM_{2.5}$ ratio. In general, the eBC/$PM_{2.5}$ ratio seemed to follow the variation of eBC (i.e., the eBC varied relatively more than $PM_{2.5}$). Like the lowest eBC concentration (Fig. 6), the lowest eBC/$PM_{2.5}$

ratio at the TR, DH, and UB sites occurred around 3 a.m. and it was about 5 %, which was close to the median eBC/$PM_{2.5}$ fraction at the RB sites (about 4.3 %). At TR1-4, there seemed to be no large seasonal variation in the eBC/$PM_{2.5}$ ratio. At TR5-6, the eBC/$PM_{2.5}$ ratio was slightly higher during the cold season, whereas at the DH, UB, and RB sites the eBC/$PM_{2.5}$ fraction was clearly higher during the cold season.

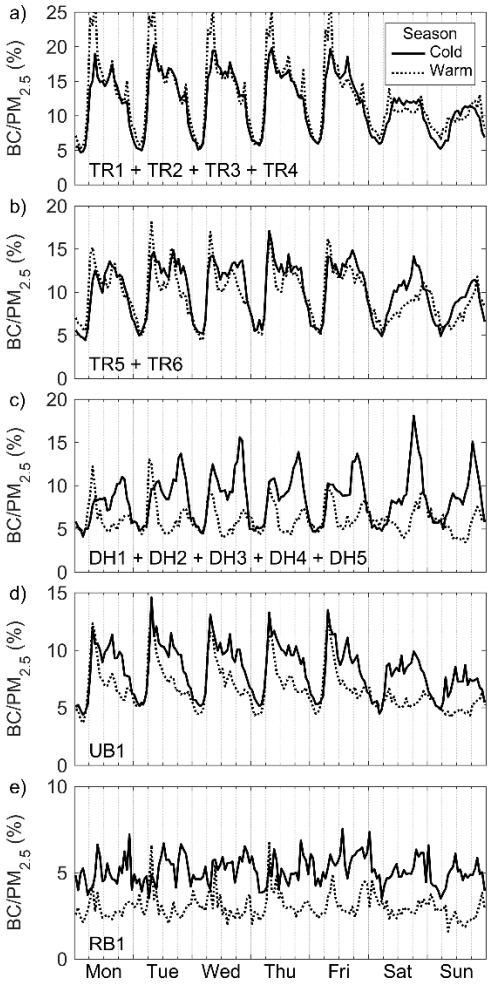


**Figure S14: Median diurnal variation of the BC/$PM_{2.5}$ fraction. Here the fraction is presented as median, since the data was noisy and the variation was not well visible with the mean values.**